Quantitative Determination of Surface Morphology of Red Blood Cell

Özlem Kocahan[1],[*]

[1]Department of Physics, Faculty of Arts and Sciences, Tekirdağ Namık Kemal University, Tekirdağ, Türkiye

Abstract − In this study, the determination of the surface morphology of red blood cell (RBC) from interferogram image obtained by quantitative phase imaging (QPI) method is presented. QPI, is an optical measurement method frequently used in recent years, allows to obtain quantitative data for different samples (cell, thin film surface, etc.). Many measurement setups at the micrometer level and with nanometer precision have been designed for quantitative surface determination. Among these, white light diffraction phase microscopy (WDPM) is a design that combines the advantages of off-axis holography-specific speed and phase sensitivity associated with common path interferometry. Interferogram image of RBCs have been formed by the WDPM setup. Analysis of this image has been carried out by Fourier transform. As a result of this analysis, three-dimensional (3D), dynamic (observable from all angles) and height-known profiles of RBCs have been created. From the height profiles, the parameters related to the morphology of RBCs as the projected surface area (PSA), diameter (D), mean corpuscular volume (MCV) and total surface area occupied by the cell (SA), have been determined quantitatively. In addition, two-dimensional images, obtained by examining blood samples with light microscopy and scanning electron microscopy (SEM), have been compared with the data achieved by WDPM. The advantages and disadvantages of WDPM and light microscopy and SEM, which are commonly used in biomedical measurements, are discussed through the results. In this way, it was possible to see the difference between QPI and traditional methods used to imaging the cell surface.

1. Introduction

Quantitative studies have come to the forefront in recent years in sciences such as biology and physics. The development of optical measurement techniques used in laboratories supports the design of more competent and cheaper measurement systems in the diagnosis and treatment phase to ensure non-invasively healthy results. Increasing the sensitivity of profilometric optical measurement systems, which are used in many fields of industry and research, is necessary for more accurate and reliable measurement (Cacace et al., 2020; Edwards et al., 2014). In the fringe projection technique used for quantitative phase imaging (QPI) in profile determination studies, the fringe pattern is projected onto the object whose height is to be measured with the help of projection and its image is recorded. From this image, the phase value for each pixel is calculated and when added together, the surface profile of the object is obtained in gradient units. This phase distribution is converted into height information using the geometry of the experimental setup (Takeda & Mutoh, 1983). When the object under investigation becomes relatively smaller, the experimental setup should also change. In 2001, Quan and colleagues used the LCD fringe projection method to obtain three-dimensional images of writing on coins (Quan et al., 2001). In the following years, interferometry was proposed for micrometer-scale measurements (Endo et al., 2005; Leonhardt, 2005; Reolon et al., 2006) and cell imaging with white light diffraction phase microscopy (WDFM) (Majeed et al., 2017; Mir et al., 2010; Popescu et al., 2008). Studies on the red blood cell (RBC) morphology with different QPI setups have increased considerably in recent years and are published in high-impact journals (Ahmadzadeh et al., 2017; Jaferzadeh & Moon, 2016; Moon et al., 2013; Singh et al., 2020).

---

[1] okocahan@nku.edu.tr

[*]Corresponding Author

RBC size, count and other morphological measurements are frequently used in the diagnosis and follow-up of many diseases by various methods (Curl et al., 2005; Lee et al., 2013; Popescu, 2011). There are several articles which have investigated RBC morphology using conventional methods (Buys et al., 2013; Mukherjee et al., 2015; Oprisan et al., 2017). In these studies, cell surface was usually imaged by atomic force microscopy (AFM) and scanning electron microscopy (SEM). These commonly used imaging techniques require a preliminary preparation of the blood sample. Although higher resolutions can be achieved with SEM and AFM imaging, the sample is damaged during measurement. QPI can provide quantitatively precise knowledge of cell structure at the cellular level (Ahmadzadeh et al., 2017). Structural parameters such as cell diameter (D), projected surface area (PSA), total surface area (SA) and mean corpuscular volume (MCV) can be calculated from the three-dimensional (3D) profile obtained by QPI (Jaferzadeh & Moon, 2016). WDPM, an interferometric technique, provides quantitative measurement of RBCs (Bhaduri et al., 2012; Pham et al., 2013; Ünal et al., 2020). A common path interferometer is an interferometer in which the sample and the reference beam propagate along the same path. In off-axis holography, it is possible to obtain the phase of an interferogram by taking only one image with a camera. There is an interferometric setup with a non-zero angle between the sample and reference beam and requires filtering spatial frequencies. WDPM is a QPI method that integrates the benefits of both the speed characteristic of off-axis holography and the phase precision related to common path interferometry (Majeed et al., 2018).

WDPM allows the determination of the RBC morphological parameters without sample preparation and non-invasive way. With this method, a sample image and a reference image are needed to calculate the 3D profile of the sample. The WDPM, which consists of an interferometer, light microscope and camera, ensures low speckle noise with white light and single-shut measurement (Bhaduri et al., 2012; Edwards et al., 2014). Phase values are calculated from an interferogram of the sample surface using various phase calculation techniques. The most widely used phase calculation method for this purpose is the Fourier transform. The height information in the interferogram is retrieved from the phase term (Takeda & Mutoh, 1983). Once the phase of each point (pixel by pixel) on the surface of the sample and the reference is determined, they are combined to obtain a 3D profile of the sample dynamically and quantitatively without damaging the sample.

In this study, three-dimensional dynamic surface profiles of RBCs have been achieved with the WDPM measurement system and the Fourier transform analysis. In the first section, the experimental setup in which interferogram image has been acquired is described in detail. In the next section, Fourier transform phase calculation method is explained and the quantitative surface profiles have been given. In addition, the light microscopy and SEM imaging procedures applied for the same blood sample are detailed and the obtained images have been compared with quantitative surface profiles. In this way, it has been possible to see the difference between the most commonly used methods and QPI, for imaging the cell surface and generating quantitative data about the morphology of RBC.

2. Materials and Methods

2.1. WDPM Method

2.1.1. Imaging with WDPM

WDPM is a system consisting of an interferometer, camera and microscope. In this technique, micrometer-scale measurements can be made by interferometry without contact with the object. In order to achieve the surface profile of RBC in a dynamic three-dimensional structure, it is first necessary to obtain interferogram images for the sample and reference.

The WDPM measurement system was equipped with a Zeiss Axio Observer A1 inverted microscope with halogen light and a Hamamatsu ORCA Flash 4.0 CMOS camera. The CMOS image sensor in this camera realizes both low noise (1.0 electrons (median) 1.6 electrons (r.m.s)) and high-speed readout (100 frames/s with 2048 pixels x 2048 pixels) at the same time, with an exposure time of 1 ms. This camera has an effective area of 13,312 mm x 13,312 mm and a pixel size of 6.5 µm. This setup was mounted on an optical table to minimize mechanical vibrations and minor disturbances in the interferometer. Figure 1 (a) shows the WDPM setup.
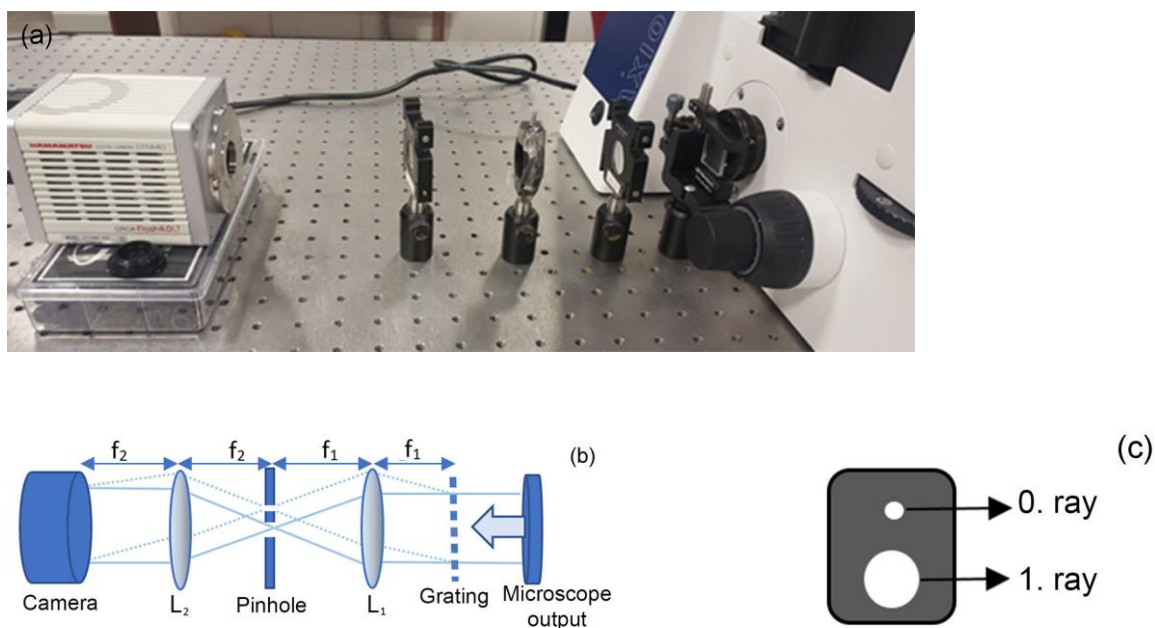
Figure 1. (a) WDPM experimental setup; (b) schematic representation of the interferometer (L_1, 60 mm focal length lens; the pinhole has two apertures with diameters of 210µm and 5 mm; L_2, 150 mm focal length lens; the camera; (c) pinhole.

First, the blood sample is spread on a slide without any preliminary preparation and covered with another slide. The sample is placed in an inverted microscope, focused and a clear image is obtained. This image is projected onto the diffraction grating from the image output at the bottom of the microscope. Different wavelengths are diffracted at different angles through the grating (110 grooves⁄mm). As shown in Figure 1(b), after passing through the diffraction grating, the rays from the microscope image plane encounter the first lens with a focal length of 60 mm. The image components incident on the Fourier plane behind the lens are filtered by a pinhole (Figure 1 (c)) having two apertures of 210 µm and 5 mm diameter. The 0th and 1st components are passed through the pinhole and encounter the second lens with a focal length of 150 mm, while the initial image is observed upside down. Component 1 passing through the 5 mm aperture and component 0 passing through the 210 µm aperture are superposed on the resulting image plane through the second lens, forming an interferometric pattern. The +1st beam is not along the optical axis and has a small angle with the 0th beam. Therefore, it generates a lateral shift. However, the amount of this shift is small enough and does not affect the generated profile. With the camera in the result image plane, a reference image without blood sample is first recorded. This reference image is used to remove impurities in the system. And then, the interferogram is generated and recorded for the blood sample. The interferometer magnifies the sample and reference image M=f2/f1=2.5 times. When taking into account with the magnification of the objective used, WDPM gives a total magnification of 157.5 for the image with a 63X objective. The RBC interferogram generated in the WDPM setup is shown in Figure 2. From this interferogram, the Fourier transform was used to calculate the surface profile showing the height at each point.
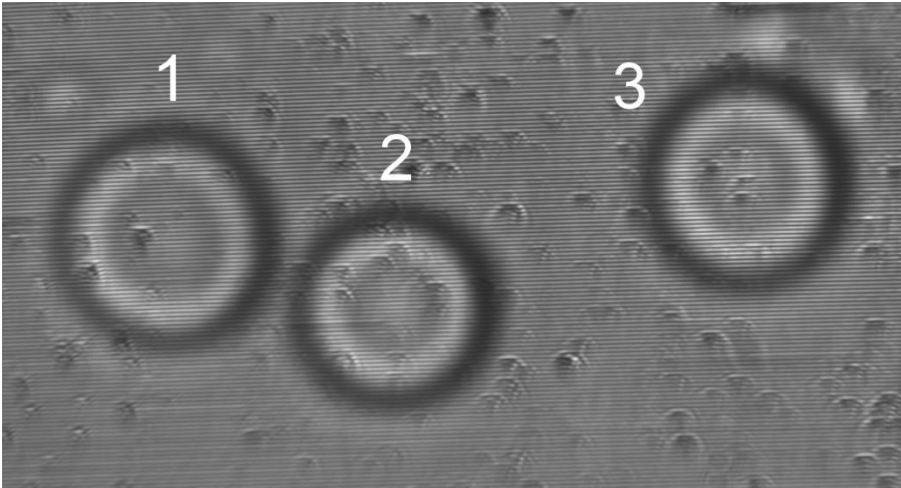
Figure 2. RBC interferogram obtained from the WDPM measurement system.

2.1.2. Phase Calculation Method with Fourier Transform

The phase term in the Fourier transform carries the height information in the images obtained from the WDPM setup. The deformed fringe pattern can be written with carrier frequency f_0, phase $\varphi(x,y)$ and amplitude $r(x,y)$ as in equation (2.1):

$$g(x,y) = \sum_{n=-\infty}^{\infty} q_n(x,y) \exp(i2\pi n f_0 x) \qquad (2.1)$$

Here $q_n(x,y) = A_n r(x,y) exp[in\varphi(x,y)]$, $f_0 = 1/p_0$ is the fundamental frequency of the monitored fringe pattern and p_0 is the fringe width. Since there is only one carrier frequency in the x-axis direction, the fringe pattern in the image is parallel to the y-axis. The 1D Fourier transform of equation (2.1) can be written as equation (2.2)

$$G(f,y) = \int_{-\infty}^{+\infty} r(x,y) \left[\sum_{-\infty}^{+\infty} A_n \exp\big(-i2\pi x(f - nf_0) + in\varphi(x,y)\big) \right] dx. \qquad (2.2)$$

This equation can be expressed as $G(f,y) = \sum_{n=-\infty}^{\infty} Q_n(f - nf_0, y)$. $G(f,y)$ and $Q_n(f,y)$ are the 1D Fourier transforms of $g(x,y)$ and $q_n(x,y)$ respectively. The spectrum of $Q_n(f - nf_0, y)$ should be separated by the carrier frequency; the first frequency component $Q_1(f - f_0, y)$ is chosen and the inverse Fourier transform is calculated as equation (2.3)

$$\hat{g}(x,y) = A_1 r(x,y) \exp\{i[2\pi f_0 x + \varphi(x,y)]\} \qquad (2.3)$$

Repeat for the case where the height is zero;

$$\widehat{g_0}(x,y) = A_1 exp\{i[2\pi f_0 x + \varphi_0(x)]\} \qquad (2.4)$$

equation (2.4) is obtained. Equation (2.3) is multiplied by the complex conjugate of equation (2.4);

$$\hat{g}(x,y)\widehat{g_0}*(x,y) = |A_1|^2 r(x,y) exp\{i[\Delta\varphi(x,y)]\} \qquad (2.5)$$

In equation (2.5), $\Delta\varphi(x,y) = \varphi(x,y) - \varphi_0(x)$ is the phase difference due to the change in height of the object at each point and $\Delta\varphi(x,y) = tan^{-1}\left[\frac{Im(\hat{g}(x,y)\widehat{g_0}*(x,y))}{Re(\hat{g}(x,y)\widehat{g_0}*(x,y))}\right]$. Thus, the height (phase difference) of each point

(pixel) on the surface from the reference plane is determined in radians and when added together, the profile of the object is achieved (Dursun et al., 2004; Takeda & Mutoh, 1983). If the same process is repeated for the reference image and the phase of the reference image is subtracted from the phase values of the image containing the RBC, the impurities and background brightness in the system are minimized.

2.1.3.   Determination of RBC Morphology

By applying the Fourier transform, the phase distribution was calculated from the interferogram obtained with the WDPM experimental setup (figure (2)) and the RBC profiles were obtained in terms of phase. This phase information was converted to height in μm using the equation (2.6) (Popescu et al., 2006).

$$Z(x,y) = \frac{\lambda \Delta \varphi(x,y)}{[2\pi|n_c - n_p|]} \tag{2.6}$$

Here, the center wavelength of the halogen lamp of the microscope is 550 nm, n_c=1.41 is the refractive index of the cell and n_p=1.34 is the refractive index of the plasma surrounding the cell. Considering the total magnification (157.5 times) provided by the camera, 63X objective and the interferometer, the size of a pixel of the raw image is 0.04x0.04 μm. Based on these calculations, the height profiles of RBCs are shown in Figure 3 at different angles.

From these height profiles, the morphological parameters of the RBCs such as the projected surface area (PSA), diameter (D), mean corpuscular volume (MCV) and the entire surface area (SA) were calculated. The first morphological parameter is the PSA, which is the area of the cell in the x-y plane (Jaferzadeh et al., 2019; Jaferzadeh & Moon, 2016). It is calculated from the equation $PSA = Np^2$, where N is the total number of pixels occupied by the cell in the x-y plane and p is the size of a pixel (0.04x0.04 μm). The diameter of the cell can be calculated by the equation $D = 2\sqrt{PSA/\pi}$ (Jaferzadeh et al., 2019; Jaferzadeh & Moon, 2016). In addition, MCV is calculated from the height profile as $MCV = p^2 \sum z(x,y)$ (Ahmadzadeh et al., 2017; Jaferzadeh & Moon, 2016). The SA of the RBC is determined from the height profile as the sum of all surface areas divided into small triangular pieces (Park et al., 2016).
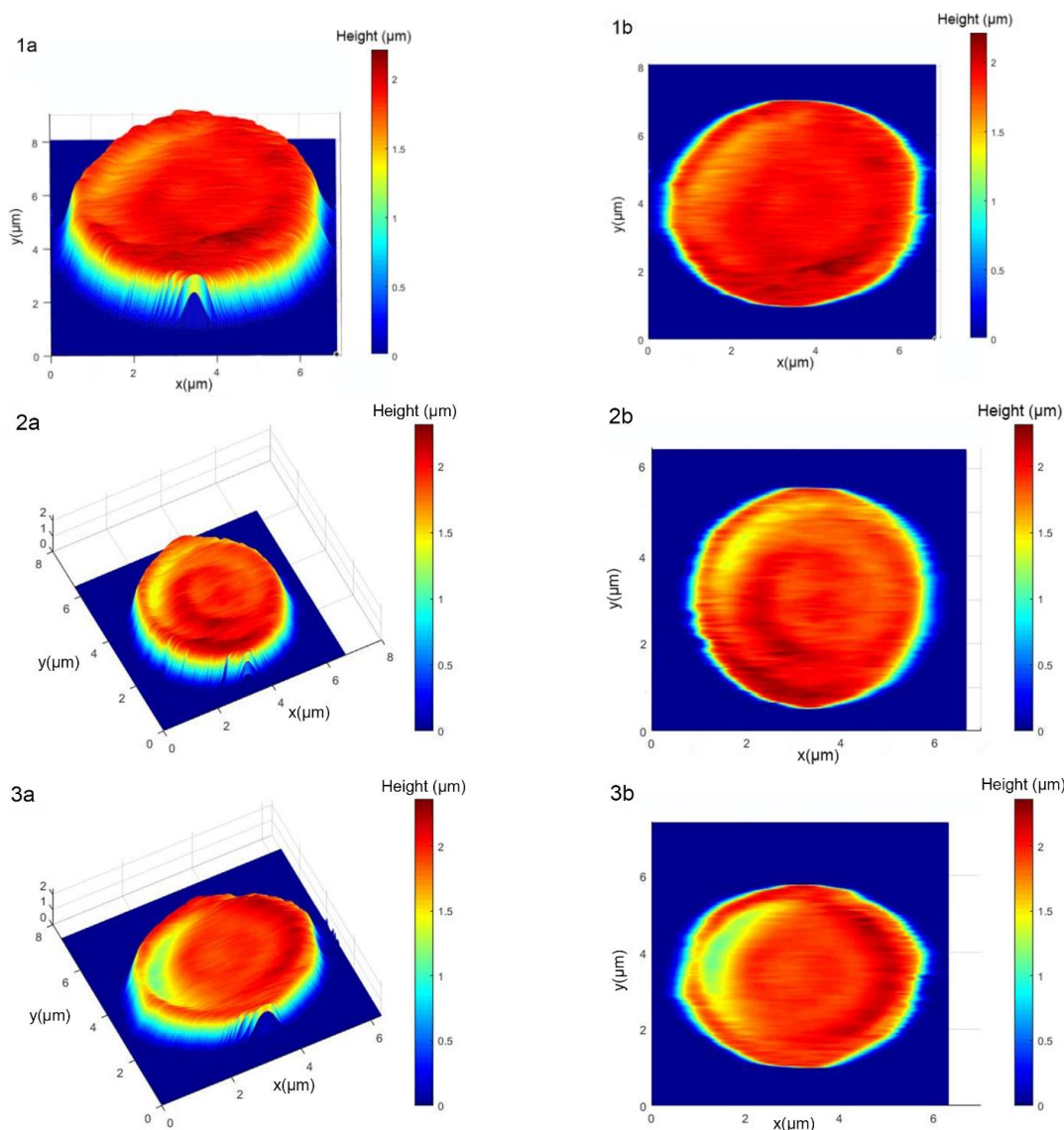
Figure 3. (a) from different angles; (b) full front view of the 3 profiles obtained by Fourier transform method from the interferogram in Figure 2 created by WDPM.

2.2. SEM Method

2.2.1 Preparation of RBCs for SEM Imaging

In order to image the blood sample with SEM, a sample preparation phase is required. This process was carried out by following these steps (Ünal et al., 2020):

a. Blood samples are collected in EDTA tubes and stored at +4 ^{0}C for one day.
b. Samples are first spread on a glass slide and washed with phosphate buffered saline (PBS.

c. The washed samples are then fixed in 2.5% glutaraldehyde with sodium cacodylate trihydrate for 120 minutes.

d. The samples are then stored in sodium cacodylate trihydrate at 4 ^{0}C.

e. After dried for examination, they are ready for SEM imaging.
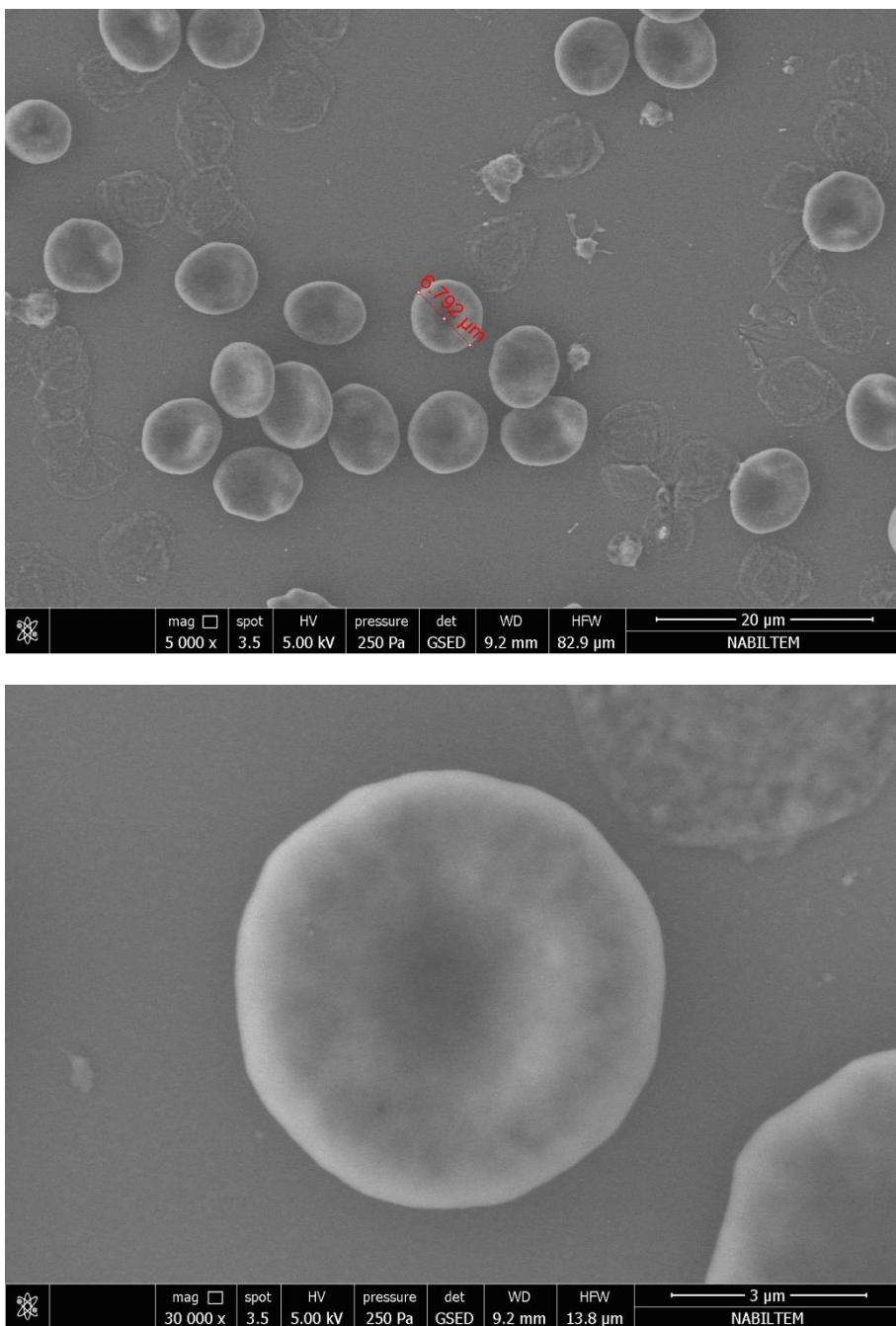
2.2.2. Imaging with SEM

Figure 4. Images of RBCs retrieved by SEM imaging

Basically, an electron microscope functions as follows; an electron source emits electrons that interact with the sample to be examined, which are then processed by the detector to produce an image. The electron source is an electron gun containing a tungsten or tungsten filament wire. A high voltage is applied to the filament, which heats the wire to a temperature of about 2700 K and releases electrons. In order for the oscillation to occur, the current must be increased as well as the voltage applied to the wire, and it is determined that the thickness of the filament to be used should be 0.125 mm on average. The oscillating electrons are guided by the anode plate, passing through lenses with electromagnetic properties and falling on the sample. Thus, the accelerated electron beam interacts with the sample and the electrons, which change their direction as a result of elastic collision with the sample atoms, are scattered back. Inelastic collisions of the electron beam with the outer orbital electrons of the sample atoms result in the formation of lower-energy Auger electrons, which allow us to obtain information about the sample surface. As a result of all these collisions, electrons that have

broken out of their orbits and lost energy form secondary electrons. Thanks to these secondary electrons coming from 10 nm below the sample surface, a high-resolution topographic image is obtained from the sample (Goldstein et al., 2018; Zhou & Wang, 2007).

Structural, topographical and morphological features and elemental analysis can be performed with SEM and samples can be monitored at different magnifications. Since, SEM gives a photography of the sample surface with scale information, has a disadvantage compared to QPI (Ahmadzadeh et al., 2017). The images obtained with SEM are not dynamic and a qualitative measurement result is obtained. In addition, the blood cells need to be subjected to a preliminary preparation process before imaging. The prepared RBCs were imaged with a FEI, Quanta FEG SEM instrument at NABILTEM at Tekirdag Namık Kemal University (figure (4)).

2.3. Imaging with Light Microscope

Blood samples were smeared onto a glass slide and covered with another slide. Without any further preparation, these sandwiched blood samples were imaged on an Inverted Axio Observer microscope using a 40X objective. Firstly, the microscope was adjusted to clarify the image and the resulting clear image of RBCs was recorded with a Hamamatsu Orca Flash 4.0 camera. In the light microscope image shown in Figure 5, RBCs were observed as biconcave in shape.

On 28.06.2022, permission was obtained from Tekirdağ Namık Kemal University Non-Interventional Clinical Research Ethics Committee for the study titled "Determination of Erythrocyte Morphologies in Multiple Sclerosis Patients by Quantitative Phase Imaging Method". The blood samples used in this study were collected from healthy volunteers of the study for which ethics committee approval was obtained.
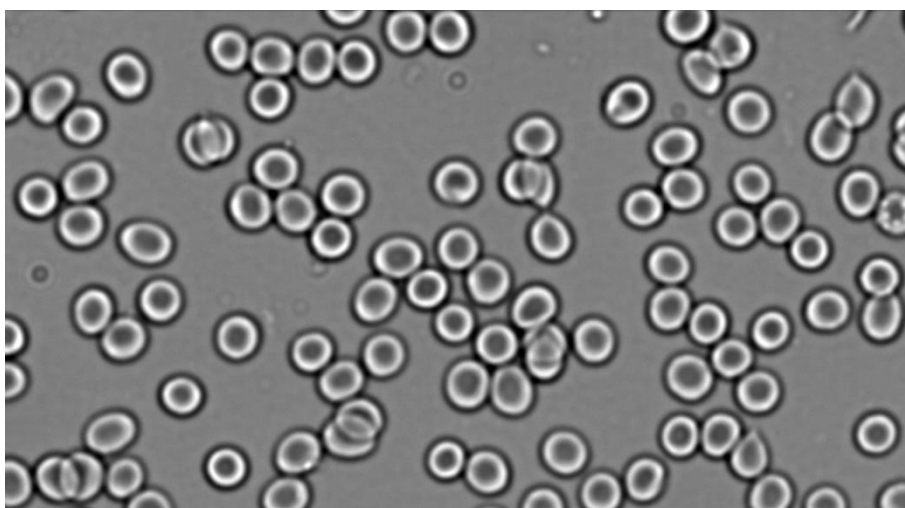

Figure 5. Light microscopy images of blood samples.

3. Results and Discussion

In order to determine the surface morphology of RBCs with the QPI technique, the WDPM experiment setup was performed as shown in Figure 1 and the interferogram image shown in Figure 2 was obtained. Phase values were calculated for each pixel of the interferogram image using Fourier transform method and these phase values were converted into height information. Thus, surface profiles of the RBCs with known height values at each point were created. These profiles are three-dimensional and dynamic, observable from any angle and quantitative. Morphological parameters for the profiles given in Figure 3: PSA=79.91 μm^2, D=5.74 μm, MCV=92.53 μm^3 and SA=131.14 μm^2 for cell 1; PSA= 71.45 μm^2, D= 4.94 μm, MCV= 83.79 μm^3 and SA= 117.68 μm^2 for cell 2; PSA= 74.99 μm^2, D= 5.38 μm, MCV= 87.85 μm^3 and SA= 123.85 μm^2 for cell 3. These values are consistent with the literature (Park et al., 2016). The samples were not subjected to any preliminary preparation while creating these profiles. One of the advantages of this technique is that the samples were imaged in the WDPM without any contact or damage. WDPM provides fast measurement, which is an advantage of off-axis holography, and is a phase-sensitive QPI method, which is an advantage of common path interferometry. In conclusion, the advantages and disadvantages of the WDPM measurement system can be listed as follows: no sample preparation is required; the measurement acquisition time is the sum of the camera

recording time (1 second) and the image analysis time (average of 1 minute, depending on the size of the image by Fourier transform); there is no contact with the sample during imaging; no sample distortion occurs. In addition, the profile obtained from WDPM images is three-dimensional and dynamic, it can be observed from any angle, it is a quantitative result with known phase and/or height values at each point, and it is possible to calculate different parameters related to morphology from the profile.

In order to compare the advantages and disadvantages of the cell profiles obtained using the WDPM method, the widely preferred SEM and light microscopy imaging were also performed.

Blood sample was first subjected to a preliminary preparation process for obtaining SEM images. Thus, the RBCs fixed on the slide were placed in the SEM device. It was observed that some RBCs were distorted during the measurement due to the pressure and temperature applied by the device (figure 4). In addition, this device scans the sample surface with an electron beam for imaging, which can damage the sample as there is contact with the sample. In the SEM image, RBC diameters were observed around 6.7 μm, but no quantitative data on the height (thickness) of the RBC could be obtained. The measurement of RBC diameter from SEM images was performed on a two-dimensional scaled photograph. Therefore, SEM can qualitatively determine the structural, morphological and topographical features of the surface of RBCs while it has the major advantage of observing samples at different magnifications with high resolution. However, it has some disadvantages; it gives a two-dimensional surface image with scale information and no height information, it is not a quantitative morphology determination technique, sample preparation is required before the imaging process, which is a disadvantage in terms of both time and cost, there is a contact with the sample, so distortion of the sample may occur due to the pressure applied inside the device during imaging.

No preparation was done for light microscopy imaging. The magnification of the light microscope is 40x and the images provide information about the shape of the RBC in general. The observation of biconcave shapes (figure 5) confirms the SEM images and the generated three-dimensional profile. With light microscopy, a large number of cells can be observed at the same time and no sample preparation is required. However, the image is in two-dimensional, contains no height information, no quantitative information can be obtained and depends on the visual interpretation of the researcher who performs the imaging and examines the image.

4. Conclusion

Using a QPI method such as WDPM, 3D height profile and morphology-related parameters of RBCs can be determined. Quantitative information can be generated with QPI measurement methods that have been developed in recent years and can provide solutions to many problems in the fields of biology, health and technology. The fact that the quantitative information to be generated with QPI can be performed without any preliminary preparation of RBCs that can be easily obtained from peripheral blood and without contact, the low cost compared to other methods will make the process easily accessible and applicable.

Acknowledgement

Author Contributions

Özlem Kocahan: Conceived and designed the analysis; collected data and performed the analysis; performed statistical analysis and wrote the paper.

Conflicts of Interest

The authors declare no conflict of interest.

References

Ahmadzadeh, E., Jaferzadeh, K., Lee, J., & Moon, I. (2017). Automated three-dimensional morphology-based clustering of human erythrocytes with regular shapes: stomatocytes, discocytes, and echinocytes. *Journal of Biomedical Optics*, 22(7), 076015. https://doi.org/10.1117/1.jbo.22.7.076015

Bhaduri, B., Pham, H., Mir, M., & Popescu, G. (2012). Diffraction phase microscopy with white light. *Optics Letters*, 37(6), 1094–1096. http://www.ncbi.nlm.nih.gov/pubmed/23292428

Buys, A. V, Van Rooy, M.-J., Soma, P., Van Papendorp, D., Lipinski, B., & Pretorius, E. (2013). Changes in red blood cell membrane structure in type 2 diabetes: a scanning electron and atomic force microscopy study. *Cardiovascular Diabetology*, *12*(1), 25. https://doi.org/10.1186/1475-2840-12-25

Cacace, T., Bianco, V., & Ferraro, P. (2020). Quantitative phase imaging trends in biomedical applications. *Optics and Lasers in Engineering*, *135*(February), 106188. https://doi.org/10.1016/j.optlaseng.2020.106188

Curl, C. L., Bellair, C. J., Harris, T., Allman, B. E., Harris, P. J., Stewart, A. G., Roberts, A., Nugent, K. a., & Delbridge, L. M. D. (2005). Refractive index measurement in viable cells using quantitative phase-amplitude microscopy and confocal microscopy. *Cytometry Part A*, *65*(1), 88–92. https://doi.org/10.1002/cyto.a.20I34

Dursun, A., Özder, S., & Ecevit, F. N. (2004). Continuous wavelet transform analysis of projected fringe patterns. *Measurement Science and Technology*, *15*(9), 1768–1772. https://doi.org/10.1088/0957-0233/15/9/013

Edwards, C., Zhou, R., Hwang, S., McKeown, S. J., Wang, K., Bhaduri, B., Ganti, R., Yunker, P. J., Yodh, A. G., Rogers, J. A., Goddard, L. L., & Popescu, G. (2014). Diffraction phase microscopy: monitoring nanoscale dynamics in materials science [Invited]. *Applied Optics*, *53*(27), G33. https://doi.org/10.1364/AO.53.000G33

Endo, T., Yasuno, Y., Makita, S., Itoh, M., & Yatagai, T. (2005). Profilometry with line-field Fourier-domain interferometry. *Optics Express*, *13*(3), 695–701. https://doi.org/org/10.1364/OPEX.13.000695

Goldstein, J. I., Newbury, D. E., Michael, J. R., Ritchie, N. W. M., Scott, J. H. J., & Joy, D. C. (2018). Scanning Electron Microscopy and X-Ray Microanalysis. In *Physicochemical Methods of Mineral Analysis*. Springer New York. https://doi.org/10.1007/978-1-4939-6676-9

Jaferzadeh, K., & Moon, I. (2016). Human red blood cell recognition enhancement with three-dimensional morphological features obtained by digital holographic imaging. *Journal of Biomedical Optics*, *21*(12), 126015. https://doi.org/10.1117/1.jbo.21.12.126015

Jaferzadeh, K., Sim, M. W., Kim, N. G., & Moon, I. K. (2019). Quantitative analysis of three-dimensional morphology and membrane dynamics of red blood cells during temperature elevation. *Scientific Reports*, *9*(1), 1–9. https://doi.org/10.1038/s41598-019-50640-z

Lee, K., Kim, K., Jung, J., Heo, J., Cho, S., Lee, S., Chang, G., Jo, Y., Park, H., & Park, Y. (2013). Quantitative Phase Imaging Techniques for the Study of Cell Pathophysiology: From Principles to Applications. *Sensors*, *13*(4), 4170–4191. https://doi.org/10.3390/s130404170

Leonhardt, K. (2005). Optical topometry of surfaces with locally changing materials, layers and contaminations Part 2: Fringe projection topometry. *Journal of Modern Optics*, *52*(10), 1367–1384. https://doi.org/10.1080/09500340512331309057

Majeed, H., Ma, L., Lee, Y. J., Kandel, M., Min, E., Jung, W., Best-Popescu, C., & Popescu, G. (2018). Magnified Image Spatial Spectrum (MISS) microscopy for nanometer and millisecond scale label-free imaging. *Optics Express*, *26*(5), 5423. https://doi.org/10.1364/OE.26.005423

Majeed, H., Sridharan, S., Mir, M., Ma, L., Min, E., Jung, W., & Popescu, G. (2017). Quantitative phase imaging for medical diagnosis. *Journal of Biophotonics*, *10*(2), 177–205. https://doi.org/10.1002/jbio.201600113

Mir, M., Ding, H., Wang, Z., Reedy, J., Tangella, K., & Popescu, G. (2010). Blood screening using diffraction phase cytometry. *Journal of Biomedical Optics*, *15*(2), 027016. https://doi.org/10.1117/1.3369965

Moon, I., Yi, F., Lee, Y. H., Javidi, B., Boss, D., & Marquet, P. (2013). Automated quantitative analysis of 3D morphology and mean corpuscular hemoglobin in human red blood cells stored in different periods. *Optics Express*, *21*(25), 30947. https://doi.org/10.1364/oe.21.030947

Mukherjee, R., Saha, M., Routray, A., & Chakraborty, C. (2015). Nanoscale Surface Characterization of Human Erythrocytes by Atomic Force Microscopy: A Critical Review. *IEEE Transactions on Nanobioscience*, *14*(6), 625–633. https://doi.org/10.1109/TNB.2015.2424674

Oprisan, B., Stoica, I., & Avadanei, M. I. (2017). Morphological changes induced in erythrocyte membrane by the antiepileptic treatment: An atomic force microscopy study. *Microscopy Research and Technique*, *80*(4), 364–373. https://doi.org/10.1002/jemt.22804

Park, H., Lee, S., Ji, M., Kim, K., Son, Y., Jang, S., & Park, Y. (2016). Measuring cell surface area and deformability of individual human red blood cells over blood storage using quantitative phase imaging. *Scientific Reports*, *6*(June), 1–10. https://doi.org/10.1038/srep34257

Pham, H. V, Edwards, C., Goddard, L. L., & Popescu, G. (2013). Fast phase reconstruction in white light diffraction phase microscopy. *Applied Optics*, *52*(1), A97. https://doi.org/10.1364/AO.52.000A97

Popescu, G. (2011). *Quantitative Phase Imaging of Cells and Tissues*. The McGraw-Hill Companies, Inc. https://www.accessengineeringlibrary.com/browse/quantitative-phase-imaging-of-cells-and-tissues

Popescu, G., Ikeda, T., Dasari, R. R., & Feld, M. S. (2006). Diffraction phase microscopy for quantifying cell structure and dynamics. *Optics Letters*, *31*(6), 775. https://doi.org/10.1364/OL.31.000775

Popescu, G., Park, Y. K., Choi, W., Dasari, R. R., Feld, M. S., & Badizadegan, K. (2008). Imaging red blood cell dynamics by quantitative phase microscopy. *Blood Cells, Molecules, and Diseases*, *41*(1), 10–16. https://doi.org/10.1016/j.bcmd.2008.01.010

Quan, C., He, X. Y., Wang, C. F., Tay, C. J., & Shang, H. M. (2001). Shape measurement of small objects using LCD fringe projection with phase shifting. *Optics Communications*, *189*(1–3), 21–29. https://doi.org/10.1016/S0030-4018(01)01038-0

Reolon, D., Jacquot, M., Verrier, I., Brun, G., & Veillas, C. (2006). Broadband supercontinuum interferometer for high-resolution profilometry. *Optics Express*, *14*(1), 128–137. https://doi.org/org/10.1364/OPEX.14.000128

Singh, V., Srivastava, V., & Mehta, D. S. (2020). Machine learning-based screening of red blood cells using quantitative phase imaging with micro-spectrocolorimetry. *Optics and Laser Technology*, *124*(December 2019). https://doi.org/10.1016/j.optlastec.2019.105980

Takeda, M., & Mutoh, K. (1983). Fourier transform profilometry for the automatic measurement of 3-D object shapes. *Applied Optics*, *22*(24), 3977. https://doi.org/10.1364/ao.22.003977

Ünal, A., Kocahan, Ö., Altunan, B., Aksoy Gündoğdu, A., Uyanık, M., & Özder, S. (2020). Quantitative phase imaging of erythrocyte in epilepsy patients. *Microscopy Research and Technique*, *December*, 1–9. https://doi.org/10.1002/jemt.23676

Zhou, W., & Wang, Z. L. (2007). Scanning Microscopy for Nanotechnology. In W. Zhou & Z. L. Wang (Eds.), *Scanning Microscopy for Nanotechnology: Techniques and Applications*. Springer New York. https://doi.org/10.1007/978-0-387-39620-0